ac susceptibility of a spherical $Nd_2Fe_{14}B$ single crystal

D.-X. Chen,* V. Skumryev, and H. Kronmüller
Max-Planck-Institut für Metallforschung, Institut für Physik, Heisenbergstrasse 1, D-7000 Stuttgart-80, Germany
(Received 16 December 1991)

The external complex ac susceptibility $\chi_e=\chi_e'-j\chi_e''$ of a spherical $Nd_2Fe_{14}B$ single crystal has been measured as a function of temperature, field amplitude, and frequency in both directions, parallel and perpendicular to the c axis. $\chi_e'(\perp)$ for $T>T_s$, the spin reorientation temperature, is due to domain-magnetization rotations (DMR's). $\chi_e'(\perp)$ for $T<T_s$ is due to comparable DMR's and domain-wall displacements (DWD's). $\chi_e'(\parallel)$ for the whole range is mainly due to DWD's. DWD's are usually enhanced by DMR's. There is an anomalous sharp $\chi_e'(\parallel)$ peak at $T=T_s$ for low fields and frequencies, which is ascribed to a technical magnetization mechanism when the first anisotropy constant equals zero. For data analyses and explanation, relations between the low-field susceptibility and the anisotropy constants, expressions of the domain-wall energy density, and a formula for χ_e'' arising from eddy currents for a metallic magnetic sphere have been derived.

I. INTRODUCTION

As a basic material of the recently developed rare-earth–iron–boron hard magnets, $Nd_2Fe_{14}B$ compounds have recently been extensively studied. There has been an agreement that at room temperature the magnetic moments lie along the tetragonal c axis and with decreasing temperature a spin-reorientation transition (SRT) from easy axis to easy cone takes place at $T=T_s\approx 135$ K, the SRT temperature. The temperature dependence of the tilting angle, which is about 30° at low temperatures, has been reported in Refs. 1–6. It is well accepted that the temperature dependence of magnetocrystalline anisotropy energy is the origin for this SRT. The anisotropy constants as functions of temperature have been reported in Refs. 3–6.

ac susceptibility technique is a powerful tool for studying magnetic phase transitions and could be very useful for analyzing transitions caused by the change in anisotropy energy. This technique has already been applied for studying SRT in strongly anisotropic materials,[7–19] including a $Ho_2Fe_{14}B$ single crystal[16] and some polycrystalline $Nd_2Fe_{14}B$ samples.[8,10,11,14,17,18] Most works gave the temperature dependence of a relative ac susceptibility in arbitrary units, so that only the possible transitions could be indicated. A few papers reported the actual values of the real part of the complex susceptibility χ' (Refs. 15–18) or both the real χ' and imaginary χ''.[19] Some equations concerning the relationship between initial susceptibility and anisotropy constants were also given,[8,14–16,18] and they were compared with the experimental data.[16,18] Moreover, the field amplitude and frequency dependences were studied in Ref. 19.

In the present work, we extend such studies to a spherical $Nd_2Fe_{14}B$ single crystal. Extending the above cited previous works, we will show that temperature, field amplitude, and frequency, as well as field-direction dependences of both χ' and χ'' can all provide important information on the anisotropy energy, domain structure, and technical magnetization process. The paper is organized as follows: In Secs. II and III we describe the experimental procedure and results. The quantitative data treatments are based on the published anisotropy constants and an ideally demagnetized state, which are given and defined in Sec. IV. In Secs. V–VII, we give a complete set of formulas which are required for such treatments. We derive formulas for the initial susceptibility as a function of the anisotropy constants for domain-magnetization rotations (Sec. V), formulas for the initial susceptibility due to domain-wall displacements, including the 180° domain-wall energy density and wall width (Sec. VI), and a formula for low-frequency eddy current χ'' (Sec. VII). In Secs. VIII and IX, we discuss the experimental data and give some conclusions.

II. SAMPLE AND MEASUREMENTS

The sample was a sphere of diameter $2a=3.5$ mm, made from a $Nd_2Fe_{14}B$ single crystal whose anisotropy constants were reported in Ref. 6. The real and imaginary components χ_e' and χ_e'' of the external complex ac susceptibility were measured during warming from $T=4.2$ to 270 K using a mutual impedance bridge with a concentric coil assembly.[20] For each run of measurements, the ac field was applied along the c axis or basal plane with a fixed amplitude H_{em} between 8 and 800 A/m and fixed or periodically changed frequencies f ranging from 1 to 1000 Hz. Before the measurements the sample was thermally demagnetized by heating it above the Curie temperature.

III. EXPERIMENTAL RESULTS

χ_e' and χ_e'' vs T curves for different field amplitudes, frequencies, and crystal orientations are given in Figs. 1–3. Some more results will be described in the course of the discussion.

For the field parallel to the c axis and $H_{em}=8$ A/m,

$f=10$ and 100 Hz, χ_e' and χ_e'' are given in Figs. 1(a) and 1(b), respectively. In order to describe the features in the frequency and temperature dependences of χ_e' and χ_e'', we divide the whole temperature interval into three ranges. In the low-temperature range below 70 K, χ_e' is very low, around 0.1, and $\chi_e''\approx 0$. For the high-temperature range, there is a χ_e' maximum around 190 K, above which χ_e' is independent of f and $\chi_e''\approx 0$. The intermediate-temperature range reveals some important characteristics: For $f=100$ Hz, χ_e' increases with T, having an inflection at $T\approx 127$ K, while χ_e' for $f=10$ Hz is obviously higher, containing a sharp peak at 127 K; correspondingly, χ_e'' shows a peak for both frequencies, the peak for 10 Hz being much higher.

χ_e' and χ_e'' for the parallel field and $H_{em}=80$ A/m, $f=10$ and 100 Hz, are given in Figs. 2(a) and 2(b), respectively. In contrast with the results for $H_{em}=8$ A/m, the high-T χ_e' is much higher and the high-T χ_e'' no longer vanishes, but both are still frequency independent. For the intermediate-temperature range, the χ_e' peak is shown for $f=1$ Hz, while the inflection for higher f develops into a dip which is also present in χ_e''.

For the field applied perpendicular to the c axis, the differences between the results for $H_{em}=8$ and 80 A/m are smaller. Figures 3(a) and 3(b) show the data for $H_{em}=80$ A/m and $f=10$, 100, and 1000 Hz. The whole temperature interval can be divided into two ranges, bounded by 127 K, where χ_e' shows a sharp maximum about 2.3. The high-temperature χ_e' is frequency independent and after a drop approaches slowly a value about 0.28, while $\chi_e''\approx 0$ holds. In the low-temperature range, χ_e' increases with temperature in several steps and shows a systematic frequency dependence, and there are several peaks or steps in the χ_e'' curves corresponding to the χ_e' steps.

IV. ANISOTROPY AND EASY DIRECTIONS

A. Magnetocrystalline anisotropy

The magnetocrystalline anisotropy energy density for a tetragonal symmetry is expressed, up to the third term, by

$$E_k=K_1\sin^2\theta+K_2\sin^4\theta+K_3\sin^4\theta\cos 4\phi\ , \tag{1}$$

where K_1, K_2, and K_3 are the anisotropy constants, θ is

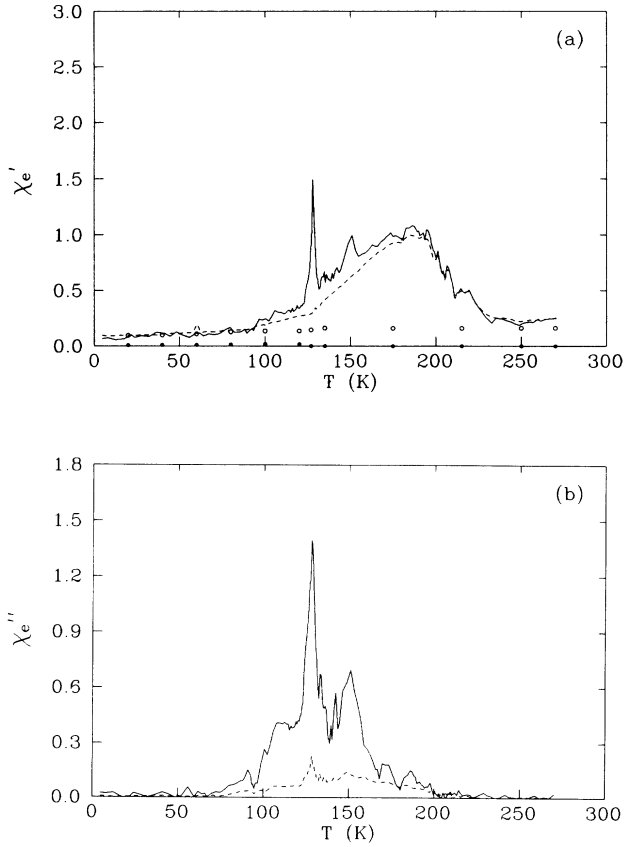

FIG. 1. Parallel (a) χ_e' and (b) χ_e'' as functions of temperature. $H_{em}=8$ A/m, $f=10$ (solid lines) and 100 Hz (dashed lines). The solid circles are the calculated DMR $\chi_{e,r}(\|)$, and the open circles are the calculated DWD $\chi_{e,w}(\|)$.

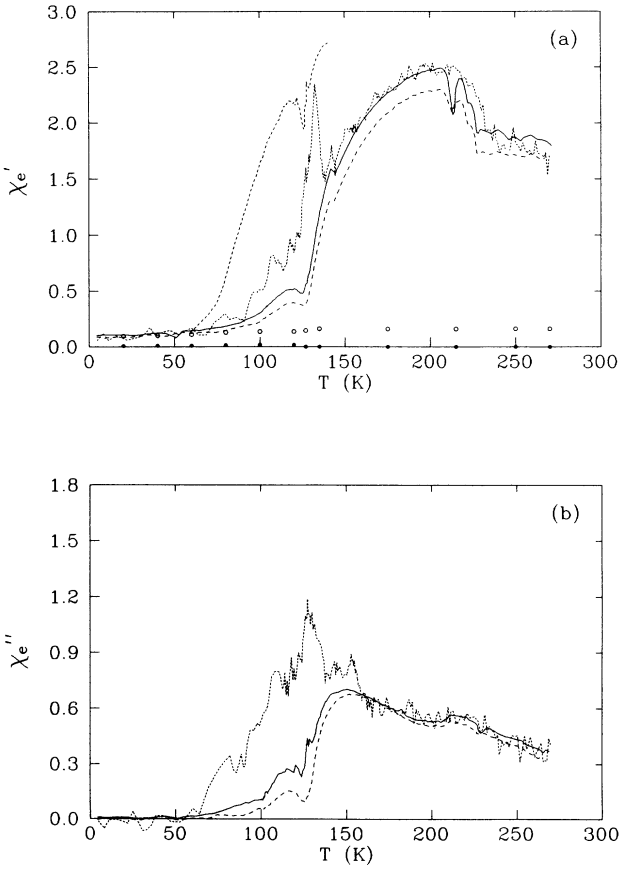

FIG. 2. Parallel (a) χ_e' and (b) χ_e'' as functions of temperature. $H_{em}=80$ A/m, $f=1$ Hz (dotted lines), 10 Hz (solid lines), and 100 Hz (dashed lines). The solid circles are the calculated DMR $\chi_{e,r}(\|)$, and the open circles are the calculated DWD $\chi_{e,w}(\|)$. In (a) the short-dashed line is for $H_{em}=240$ A/m and $f=1$ Hz.

the zenithal angle between the magnetization direction and c axis, [001], and ϕ is the azimuthal angle from the a direction [100].

For $Nd_2Fe_{14}B$ crystals the anisotropy constants as functions of temperature have been measured by several authors.[3–6] We use here for K_1 and K_2 Hock's[6] results, since his sample was taken from the same crystal as ours. For K_3 we have to use the data of Otani, Miyajima, and Chikazumi,[4] since they have made direct torque measurements on it, although the values of their low-temperature K_1 and K_2 are only about $\frac{1}{3}$ of those given by Hock.

The three constants as functions of temperature are shown in Fig. 4. With increasing temperature, K_1 increases from negative to positive value. It equals zero at around 127 K and stays almost constant, around 4.8 MJ/m^3, between 200 and 270 K. K_2 is always positive; it decreases from 50 MJ/m^3 at 20 K to 0.8 MJ/m^3 at 290 K and crosses the K_1 curve at 200 K. K_3 is rather small, with a value of 2.5 MJ/cm^3 at 4.2 K and almost vanishing above 100 K.

B. Easy directions

If only accounting for K_1 and K_2 in Eq. (1), we will have three cases, namely, easy axis, easy cone, and easy plane, depending on the values of K_1 and K_2. However, K_3 cannot be neglected for the low-field domain-magnetization rotation (DMR) susceptibility calculation. Correspondingly, we can only generally talk about easy directions.

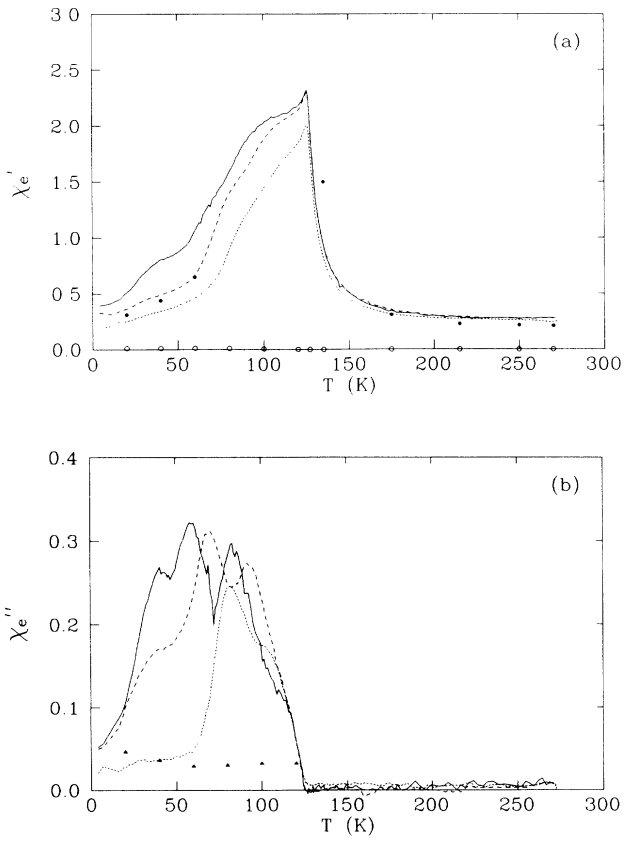

FIG. 3. Perpendicular (a) χ_e' and (b) χ_e'' as functions of temperature. $H_{em}=80$ A/m, $f=10$ Hz (solid lines), 100 Hz (dashed lines), and 1000 Hz (dotted lines). The solid circles are the calculated DMR $\chi_{e,r}(\perp)$, the open circles are the calculated DWD $\chi_{e,w}(\perp)$, the solid triangles are the calculated eddy-current $\chi_{e,\mathrm{eddy}}(\perp)$ for 1000 Hz.

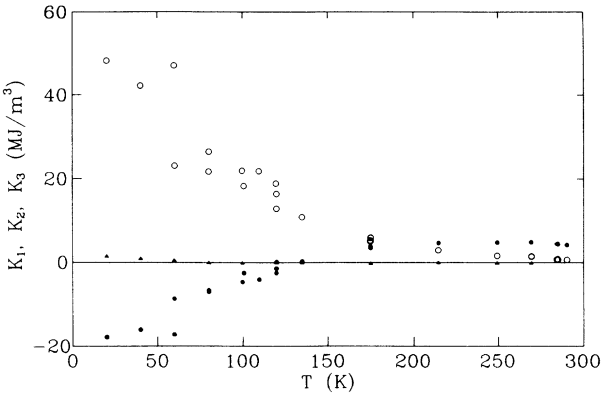

FIG. 4. K_1 (solid circles), K_2 (open circles), and K_3 (solid triangles) as functions of temperature for $Nd_2Fe_{14}B$ (Refs. 6 and 4).

The easy directions can be easily derived from the condition of $\partial E_k/\partial\theta=0$, $\partial^2 E_k/\partial\theta^2>0$ and $\partial E_k/\partial\phi=0$, $\partial^2 E_k/\partial\phi^2>0$. Writing the easy direction as (θ_0,ϕ_0) and remembering the direction opposite to (θ_0,ϕ_0) to be also an easy direction, we have the following cases which are useful for the present material.

(a) For $K_1>0$ and $K_2-|K_3|>-K_1$,

$$\theta_0=0\ . \tag{2}$$

(b) For $K_1<0$, $K_3>0$, and $K_2-K_3>-K_1/2$,

$$\sin\theta_0=\pm[-K_1/2(K_2-K_3)]^{1/2}\ , \tag{3a}$$

$$\phi_0=\pm\pi/4\ . \tag{3b}$$

Case (a) is for $T>T_s$, where T_s is the temperature corresponding to $K_1=0$, and there are two easy directions of $\theta_0=0$ and π. Case (b) is for $T<T_s$, and there are eight easy directions of $(\theta_0,\pm\pi/4)$, $(\theta_0,\pm\pi/4+\pi)$, $(\theta_0+\pi,\pm\pi/4)$, and $(\theta_0+\pi,\pm\pi/4+\pi)$, where θ_0 is calculated from Eq. (3a).

V. LOW-FIELD SUSCEPTIBILITY FROM DMR

A. Demagnetized state

In order to calculate low-field DMR susceptibility, a domain structure has to be defined. This structure is assumed to guarantee an ideal demagnetized state where the local magnetic moments are distributed with an equal probability in all the easy directions. The actual domain structure may be different from this ideal one, but the results calculated from this state can be a useful reference for data analyses.

We only derive formulas for the applied field parallel and perpendicular to the c axis. With the domain structure defined above, the direction dependence of low-field DMR susceptibility should have a uniaxial anisotropy;

i.e., it is a function of only the zenithal angle θ_H of the field, independent of its arimuthal angle ϕ_H, provided that the polar axis is chosen to be the c axis. Therefore the derivation of susceptibility perpendicular to the c axis can be done for a particular direction that is easy to be treated.

We will not consider demagnetizing effects in the calculation, so that the susceptibility is defined by $\chi=(\partial M/\partial H)_{M=0}$, where H is the internal field. In the following, subscripts h and l are used to stand for $T>T_s$ and $<T_s$, and r and w for DMR's and domain-wall displacements (DWD's), respectively.

B. Perpendicular χ for $T>T_s$

In this case, when $H=0$, two halves of magnetic moments are along equivalent easy directions $\theta_0=0$ and π, so that we can assume the applied field to be along the x direction and all the moments to be along the z direction. The total-energy density in the $\phi=0$ plane is

$$E=E_k+E_m$$
$$=K_1\sin^2\theta+(K_2+K_3)\sin^4\theta-\mu_0M_sH_x\sin\theta\ , \quad (4)$$

where E_m is the energy density of the field–magnetic-moment interaction and M_s is the spontaneous magnetization. The condition of $\partial E/\partial\theta=0$, $\partial^2E/\partial\theta^2>0$ at $\theta=\theta_0=0$ leads to a relation between the equilibrium θ and H_x as

$$\sin\theta=\frac{\mu_0M_s}{2K_1}H_x\ , \quad (5)$$

which is valid for $\theta\ll1$. Since $M_x/M_s=\sin\theta$, we obtain from Eq. (5) that

$$\chi_{rh}(\perp)=\chi_x=\frac{M_x}{H_x}=\frac{\mu_0M_s^2}{2K_1}\ , \quad (6)$$

which is the perpendicular DMR susceptibility.

C. Perpendicular χ for $T<T_s$

In this case the magnetic moments at $H=0$ are uniformly distributed in eight easy directions. The simplest treatment can be done by assuming the field to be applied in the [110] direction, written as H_{xy}. The moments with directions of $(\theta_0,\pi/4)$, $(\theta_0,\pi/4+\pi)$, $(\theta_0+\pi,\pi/4)$, and $(\theta_0+\pi,\pi/4+\pi)$ are energetically equivalent and can rotate in the plane of $\phi=\pi/4$; the moments in the rest four directions are also equivalent and can rotate only along the "easy-cone" surface. (The cone is now not perfect, and its tilting angle, corresponding to a minimum energy, changes with ϕ.) For calculation, we assume a half of the moments to be along $(\theta_0,\pi/4)$ and another half along $(\theta_0,-\pi/4)$. The easy directions and magnetization rotations are shown in Fig. 5.

For the first set of moments, we have, in the $\phi=\pi/4$ plane,

$$E=E_k+E_m$$
$$=K_1\sin^2\theta+(K_2-K_3)\sin^4\theta-\mu_0M_sH_{xy}\sin\theta\ . \quad (7)$$

Its equilibrium θ is obtained by the condition of $\partial E/\partial\theta=0$, $\partial^2E/\partial\theta^2>0$ to satisfy

$$2K_1\sin\theta+4(K_2-K_3)\sin^3\theta-\mu_0M_sH_{xy}=0\ , \quad (8)$$

from which and using Eq. (3a) we obtain the first contribution to the susceptibility χ_{xy} as

$$\chi_{xy1}=\frac{M_s}{2}\left.\frac{\partial\sin\theta}{\partial H_{xy}}\right|_{\theta=\theta_0}=-\frac{\mu_0M_s^2}{8K_1}\ , \quad (9)$$

where a weight $\frac{1}{2}$ has been included.

For the second set of moments, we have, close to the easy direction $(\theta_0,-\pi/4)$, that

$$E=E_k+E_m$$
$$=K_1\sin^2\theta_0+K_2\sin^4\theta_0+K_3\sin^4\theta_0\cos4\phi$$
$$-\mu_0M_sH_{xy}\sin\theta_0(\phi+\pi/4)\ . \quad (10)$$

The equilibrium ϕ is obtained by $\partial E/\partial\phi=0$, $\partial^2E/\partial\phi^2>0$, and it satisfies

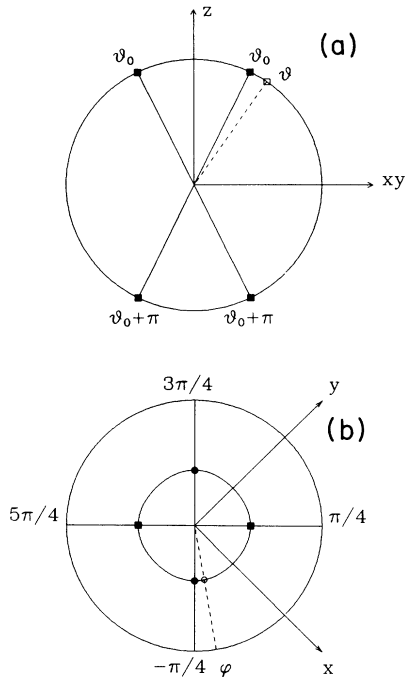

FIG. 5. Easy directions for $T<T_s$. The K data in Table I at $T=20$ K are used as an example. (a) Four energetically equivalent easy directions symbolized by solid squares on the unitary circle in the $\phi=\pi/4$ plane. When field is applied in the xy direction [110], magnetization in the $(\theta_0,\pi/4)$ direction rotates to the $(\theta,\pi/4)$ direction, symbolized by the open square (see Sec. V B). (b) Two energetically equivalent easy directions symbolized by solid circles on the $\theta<\pi/2$ surface of the unitary sphere, which is projected to the $\theta=\pi/2$ surface. The other two equivalent directions are not shown, which can be marked on the surface of $\theta>\pi/2$. The solid squares correspond to the upper two directions in (a). When field is applied in the [110] direction, magnetization in the $(\theta_0,-\pi/4)$ direction rotates to the ϕ direction, symbolized by the open circle (see Sec. V C). The loop through the symbols, which is not a perfect circle, is the cross section of the "easy cone" to the unitary sphere.

$$\sin 4\phi = -\frac{\mu_0 M_s H_{xy}}{4K_3 \sin^3\theta_0} . \quad (11)$$

For ϕ close to $-\pi/4$, this leads to

$$\Delta\phi = \phi + \pi/4 = \frac{\mu_0 M_s H_{xy}}{16K_3 \sin^3\theta_0} . \quad (12)$$

The second contribution to χ_{xy} is then obtained using Eq. (3a) and considering a weight $\frac{1}{2}$ as

$$\chi_{xy2} = \frac{M_s \sin\theta_0 \Delta\phi}{2} \frac{\partial \Delta\phi}{\partial H_{xy}} = \frac{\mu_0 M_s^2}{32K_3 \sin^2\theta_0} = -\frac{\mu_0 M_s^2 (K_2 - K_3)}{16K_3 K_1} . \quad (13)$$

The total perpendicular DMR susceptibility is finally

$$\chi_{rl}(\perp) = \chi_{xy} = \chi_{xy1} + \chi_{xy2} = -\frac{\mu_0 M_s^2 (K_2/K_3 + 1)}{16K_1} . \quad (14)$$

D. Parallel susceptibility for $T > T_s$

In this case the magnetic torque acted by H_z on the moments is zero, so that the DMR susceptibility is

$$\chi_{rh}(\parallel) = \chi_z = 0 . \quad (15)$$

E. Parallel susceptibility for $T < T_s$

In this case the moments in all the easy directions are equivalent. We have

$$E = E_k + E_m = K_1 \sin^2\theta + (K_2 - K_3)\sin^4\theta - \mu_0 M_s H_z \cos\theta . \quad (16)$$

The equilibrium equation is

$$2K_1 \cos\theta + 4(K_2 - K_3)\sin^2\theta \cos\theta + \mu_0 M_s H_z = 0 , \quad (17)$$

from which we obtain, using Eq. (3a),

$$\chi_{rl}(\parallel) = \chi_z = M_s \left. \frac{\partial \cos\theta}{\partial H_z} \right|_{\theta=\theta_0} = \frac{\mu_0 M_s^2}{4K_1 + 8(K_2 - K_3)} . \quad (18)$$

VI. DWD SUSCEPTIBILITY

A. General expressions

The DWD susceptibility is more complicated than the DMR one. For the studied material with large K_1 and/or K_2, most domain walls should be 180° walls. In this case, in the ideal demagnetized state defined above, the DWD susceptibility should be determined by the area of mobile walls, directions of the domain magnetizations relative to the field direction, domain-wall energy density γ_B, and M_s.

Following classical technical magnetization models,[21] we have for 180° walls that

$$\chi_w(\perp) = k_\perp M_s^2 \gamma_B^{-1} \sin^2\theta_0/2 , \quad (19)$$

$$\chi_w(\parallel) = k_\parallel M_s^2 \gamma_B^{-1} \cos^2\theta_0 , \quad (20)$$

where $k_\perp$ and $k_\parallel$ are constants depending on the area of mobile walls and the pinning mechanism. If the same walls with the same pinning mechanism are involved for both field directions, we should have $k_\perp/k_\parallel = 1$.

B. Domain-wall energy density and width

For 180° domain walls of the present material, the domain-wall energy density γ_B is a function of K_1, K_2, and K_3. We derive it following the procedures given in Refs. 21 and 22. Assuming A to be the exchange constant and, for simplicity, defining

$$K_2' = K_2 - |K_3| , \quad (21a)$$

$$K_{12} = K_1/K_2' , \quad (21b)$$

we have, for $T \geq T_s$, i.e., $K_1 \geq 0$, $K_2' \geq 0$,

$$\gamma_B = 2\sqrt{AK_2'} \int_0^\pi (K_{12}\sin^2\theta + \sin^4\theta)^{1/2} d\theta = 2\sqrt{AK_2'} \left[\sqrt{K_{12}} + (K_{12}+1)\sin^{-1}\sqrt{1/(K_{12}+1)}\right] , \quad (22)$$

and, for $T \leq T_s$, i.e., $K_2' \geq 0$, $-1 \leq K_{12} \leq 0$,

$$\gamma_B = 2\sqrt{AK_2'} \int_{\theta_0}^{\theta_0+\pi} (K_{12}\sin^2\theta + \sin^4\theta + K_{12}^2/4)^{1/2} d\theta , \quad (23)$$

where θ_0 is calculated from Eq. (3a). This integration can be performed numerically by a computer. If an effective anisotropy constant is defined as

$$K_{\text{eff}} = K_1 + K_2' = K_1 + K_2 - |K_3| , \quad (24)$$

we can write Eqs. (22) and (23) as

$$\gamma_B = w\sqrt{AK_{\text{eff}}} , \quad (25)$$

where w is a function of K_{12}. We have $w = \infty$, π, $\sqrt{2} + \pi/\sqrt{2}$, and 4 for $K_{12} = -1$, 0, 1, and ∞, respectively.

The domain-wall width δ_B can be traditionally defined as the distance across which the atomic moment rotates uniformly 180° with the changing speed equal to the calculated one at the wall center. Following Refs. 21 and 22, it can be derived for the whole temperature range that the 180° domain-wall width is given by the expression

$$\delta_B = \pi\sqrt{A/K_{\text{eff}}} . \quad (26)$$

VII. LOW-FREQUENCY EDDY-CURRENT SUSCEPTIBILITY FOR A FERROMAGNETIC SPHERE

A. Eddy-current loss power and loss per cycle

As first approximation, a conducting magnetic sphere in ac applied field $H_e(t) = H_{em}\cos 2\pi f t$ has a uniform

magnetic induction $B(t)=B_m\cos(2\pi ft-\delta_b)$, where δ_b is a phase delay, at low frequency f. From Faraday's law and Ohm's law, the ϕ component of the eddy-current density at the point (r,θ,ϕ), where r, θ, and ϕ are the polar coordinates of the point with the field along $\theta_H=0$, is

$$J_\phi(r,\theta,\phi)=-\frac{r\sin\theta}{2\rho}\frac{dB(t)}{dt}\ , \tag{27}$$

where ρ is the resistivity of the material. The instantaneous loss power is

$$P(t)=\int_V J_\phi^2\rho\,dv=\frac{2\pi a^5}{15\rho}\left[\frac{dB(t)}{dt}\right]^2\ , \tag{28}$$

where a is the radius of the sphere and the integration has been performed over the sphere volume V. The loss per cycle of magnetization is then

$$W=\int_0^{1/f}P(t)dt=\frac{\pi^2a^2fB_m^2V}{5\rho}\ . \tag{29}$$

B. Eddy-current χ_e''

The loss per cycle equals the work done by the applied field H_e to the sphere in one cycle of magnetization M, which is

$$W=V\mu_0\oint H_e\,dM=V\pi\mu_0\chi''_{e,\text{eddy}}H_{em}^2\ . \tag{30}$$

Comparing Eqs. (29) and (30), we obtain

$$\chi''_{e,\text{eddy}}=\frac{\pi a^2fB_m^2}{5\rho\mu_0H_{em}^2}\ . \tag{31}$$

From the definition of magnetic induction, $B=\mu_0(H+M)$, and demagnetizing field $H_d=-NM=-M/3$, we have

$$B_m=\mu_0(2M_m/3+H_{em})\ , \tag{32}$$

from which it follows

$$B_m/H_{em}=\mu_0(2\chi'_e/3+1)\ , \tag{33}$$

where the low-frequency M_m/H_{em} has been written as χ'_e. Substituting Eq. (33) into Eq. (31), we obtain the final equation for the eddy-current χ''_e as

$$\chi''_{e,\text{eddy}}=\frac{\pi a^2f\mu_0(2\chi'_e/3+1)^2}{5\rho}\ . \tag{34}$$

Our calculations are based on uniform magnetization. Considering the domain structure and nonuniform magnetization process, the results will be modified. However, Eq. (34) can be a useful reference for the ac susceptibility analysis.

VIII. DISCUSSION

A. General description of DMR and DWD susceptibility

From the calculation in Secs. V and VI, the contributions of DMR's and DWD's to the total χ' should be as follows. When $T>T_s$, χ' is due only to DMR's or DWD's if the field is perpendicular or parallel to the c axis, respectively, as given by Eqs. (6) and (20). If $T<T_s$, χ' in both directions will have two contributions. For the perpendicular case, the DMR contribution is calculated by Eq. (14), while the DWD one by Eq. (19). For the parallel case, the DMR and DWD contributions are calculated from Eqs. (18) and (20), respectively.

B. DMR susceptibility calculations

To calculate DMR susceptibilities from Eqs. (6), (14), and (18), the values of μ_0M_s, K_1, K_2, and K_3 are required. Table I lists such data, obtained from Refs. 6 and 4 directly or by averaging or interpolating the original data. $\chi_{rh}(\perp)$, $\chi_{rl}(\perp)$, and $\chi_{rl}(\parallel)$ are calculated from the listed data. In order to compare them with the measured results χ'_e, a demagnetizing conversion is performed using a general formula for the relation between the corresponding external χ'_e and internal χ' (this formula is valid for $\chi''\ll\chi'$ when χ' is very close to its dc value):

$$\frac{1}{\chi'_e}=\frac{1}{\chi'}+\frac{1}{3}\ , \tag{35}$$

where the last term is the demagnetizing factor N for a

TABLE I. Spontaneous magnetization, anisotropy constants (Ref. 6), resistivity in the basal plane (Ref. 23), and other quantities derived from them and the experimental data (see text).

T (K)	20	40	60	80	100	120	135	175	215	250	270
μ_0M_s (T)	1.84	1.84	1.83	1.82	1.80	1.79	1.77	1.75	1.72	1.68	1.66
K_1 (MJ/m^3)	−18	−16	−13	−6.8	−3.5	−1.2	0.4	3.6	4.7	4.8	4.9
K_2 (MJ/m^3)	48	42	35	24	20	18	11	5.5	3.0	1.6	1.5
K_3 (MJ/m^3)	1.6	1.0	0.6	0.1	0.0	0.1	0.1	−0.1	0.1	0.0	0.0
χ_{xy1}	0.07	0.08	0.10	0.19	0.36	1.10					
χ_{xy2}	0.27	0.43	0.73								
$\chi_{e,r}(\perp)$	0.31	0.44	0.65				1.5	0.31	0.23	0.22	0.21
$\chi_{e,r}(\parallel)\times10^3$	9	10	12	16	18	18	0	0	0	0	0
w	3.05	3.05	3.04	3.00	3.00	3.07	3.19	3.54	3.72	3.83	3.84
$\chi_{e,w}(\parallel)\times10^3$	96	101	110	130	137	138	163	162	162	163	163
$\chi'_{e,w}(\perp)\times10^3$	12	13	13	11	16	11	0	0	0	0	0
ρ (10^{-8} $\Omega\,m$)	7	10	14	20	28	36	41	49	56	58	62
$\chi_{e,\text{eddy}}$ ($\perp$, 1 kHz)$\times10^3$	47	37	30	31	33	33					

sphere. The $\chi_{e,r}(\perp)$ and $\chi_{e,r}(\parallel)$ data thus obtained are listed in Table I and plotted in Figs. 1(a), 2(a), and 3(a) by solid circles.

To have a comparison between the DMR susceptibilities from the θ and ϕ rotations, χ_{xy1} and χ_{xy2} are also listed in Table I. We can see that with increasing temperature, the ratio of the latter to the former increases from 4 at 20 K to 7 at 80 K. This means that the DMR's in the basal plane have a dominant contribution to the perpendicular DMR susceptibility at low temperatures.

C. Perpendicular susceptibility

According to Fig. 3(a), the perpendicular case, the agreement between χ'_e and the calculated external DMR susceptibility $\chi_{e,r}(\perp)$ is good at higher temperatures. A deviation of the data point at $T=135$ K away from the curves is believed to be due to the measuring error in temperature (within 2 K) and in K_1 (around 1.2 MJ/m^3, as can be seen from the scattering of the data at 120 K in Fig. 4). This means that the perpendicular susceptibility is almost fully attributed to DMR's for $T>T_s$. For $T<T_s$ the three calculated points lie between the curves for $f=100$ and 1000 Hz, suggesting that there are both contributions from DMR's and DWD's in this region. Since the perpendicular DMR susceptibility calculated from Eqs. (6) and (14) diverges at $K_1=0$, T_s can be defined as the temperature, around 127 K, where χ'_e takes its maximum.

We observe in Fig. 3(b) that $\chi''_e\approx 0$ for $T>T_s$, the pure DMR region. For $T<T_s$, where both DMR's and DWD's exist, χ''_e is rather high. These facts further suggest that the nonzero χ''_e is due to DWD's. The partial χ'_e due to DWD's is mainly present at lower frequencies; it decreases with increasing f, so that the high-f susceptibility χ'_e is close to the values calculated for DMR's. We will further argue in Sec. VIII H that the actual DMR χ'_e is lower than the data for 1000 Hz and that the calculated values are overestimated; i.e., the K_3 given in Table I has a minus error.

D. Parallel susceptibility

In the parallel case [Figs. 1(a) and 2(a)], the calculated $\chi_{e,r}(\parallel)$ is zero for $T>T_s$, the pure DWD region, where χ'_e is very high. Although this $\chi_{e,r}(\parallel)$ is not zero for $T<T_s$, it is almost negligible in comparison with the χ'_e data. Therefore the parallel χ'_e is almost completely due to DWD's in the whole temperature range.

By comparing the data with Eq. (20), we find that the temperature dependence of χ'_e cannot be totally explained by the change in M_s and γ_B. In order to make such a comparison, we calculate w and $\chi_{e,w}(\parallel)$ using Eqs. (20), (22)–(25), and (35) from the data of M_s and K's given in Table I. The data for $\chi_{e,w}(\parallel)$ are normalized so that the experimental data at low temperatures are well fitted by them. The results are also listed in Table I (except for $T=T_s$, where both values are 3.14 and 0.146, respectively) and plotted in Figs. 1(a) and 2(a) as open circles.

According to Table I, w smoothly changes with temperature, from about 3 when $T<T_s$ to 3.84 when $T=270$ K. In Fig. 1(a), after fitting the low-temperature data, the calculated $\chi_{e,w}(\parallel)$ data are very close to the experimental curves in high-temperature regions, but there is a large difference at intermediate temperatures, where the experimental data are much higher, including a χ'_e peak (10 Hz) or an inflection point (100 Hz) at $T=T_s$. In Fig. 2(a) the experimental data are much larger than the calculated ones even for the high-temperature range. The peak at $T=T_s$ and low frequency (1 Hz) becomes broad, while the inflection at higher frequencies becomes a dip.

It turns out that $k_\parallel$ is a function of temperature. For lower fields it is almost constant at low and high temperatures, but increases significantly in the intermediate-temperature region, including a peak at $T=T_s$. At higher field the increase of χ'_e at high temperatures suggests the presence of hysteresis, since the corresponding χ''_e is also high and frequency independent.

E. DWD susceptibility enhanced by DMR's

If $k_\parallel(T)=k_\perp(T)$, we can calculate the partial DWD susceptibility for the perpendicular case at $T<T_s$ from the parallel χ'_e data, which are, as explained above, almost exclusively determined by DWD's. The formula is obtained from Eqs. (19), (20), and (3a) as

$$\chi'_w(\perp)=\frac{-K_1\chi'_w(\parallel)}{4(K_2-K_3)+2K_1} . \tag{36}$$

The results are listed as $\chi'_{e,w}(\perp)$ (we put a prime to identify it to be calculated from experimental data) in Table I and plotted in Fig. 3(a) by open circles. We can see that this contribution is negligible when compared with the measured χ'_e data. Since quite a large fraction of perpendicular χ'_e is due to DWD's in this temperature region, we may conclude that $k_\perp$ is much larger than $k_\parallel$ below T_s.

We name this phenomenon "DWD susceptibility enhanced by DMR's." The reasons are as follows: The fact that the total susceptibility is larger than the sum of the two individual DMR and DWD contributions should be due to the interaction between both. The DMR susceptibility is determined by the magnetic energy in the whole sample volume, while the DWD susceptibility has a local nature. Therefore, although DWD's can enhance DMR's in some ways, the strength of the enhancement to the DMR susceptibility must be small. On the contrary, the influence of DMR's can be everywhere in the sample, so that they can enhance the DWD susceptibility to a large extent.

A remarkable phenomenon for the parallel susceptibility can be observed in Fig. 2(a). There is a large dip in χ'_e (≈ 0.04) around 127 K in the curves for $H_{em}=80$ A/m and $f=10$ and 100 Hz, and it is as large as 0.25 (or 2.5 for χ' after a demagnetizing correction) for $H_{em}=240$ A/m and $f=1$ Hz. This dip obviously corresponds to that in the parallel DMR susceptibility. However, as shown by the solid circles in the same figure, the latter is small (<0.02). This observed χ'_e dip is due to DMR's and mainly to the DWD's enhanced by DMR's, especially for higher fields. Hence at least part of the origins for

the large $k_\perp$ at $T<T_s$ can be attributed to a DMR-enhanced DWD susceptibility.

F. Parallel χ'_e peak

There is a sharp peak at $T\approx 127$ K in the parallel χ'_e curves for $H_{em}=8$ A/m and $f=10$ Hz [Fig. 1(a)] and $H_{em}=80$ A/m and $f=1$ Hz [Fig. 2(a)]. Increasing H_{em} to 240 A/m reduces the peak appreciably [Fig. 1(a)]. Further increasing H_{em} to 800 A/m finally eliminates it (data not shown). It was also absent at $H_{em}=0.8$ A/m and $f=100$ Hz (data not shown).

From the above calculations, the DMR susceptibility should be zero at $T>T_s$ and 0.018 at T a little below T_s. The DWD susceptibility should change smoothly when T passes through T_s. Therefore this peak cannot be explained by DMR's and DWD's without interaction.

We note that the peak is located at T_s, where $K_1=0$, and this provides a hint for its interpretation. For the studied sample with high anisotropy, the elementary magnetic moments in the domains should in general be parallel to the easy directions. However, there is an exception; when $K_1=0$ at $T=T_s$, the anisotropy energy around the c axis is very small, so that the magnetic moments can lie within a certain angle around the c axis with almost the same energy. This can be realized by calculating the θ dependence of the second term with a factor of $\sin^4\theta$ in Eq. (1). For example, when $\theta=5°$, 10°, and 15° this term is $5.8\times10^{-5}K_2$, $9.1\times10^{-4}K_2$, and $4.5\times10^{-3}K_2$, respectively. As a consequence, the domain magnetizations will align not only along the c axis; their directions can be within a considerable range of angles θ. Such domains can rotate in the parallel ac field. However, these DMR's still cannot give a susceptibility peak, since $\cos\theta$ is very close to unity in the parallel case and the M_z component should be close to zero. On the other hand, the domain-wall energy density is large at $T=T_s$, regardless of a zero K_1. A large susceptibility from DWD's can be realized only when the wall displacements do not change or change negligibly the total wall area, since otherwise the domain-wall energy will change appreciably because of a large γ_B at T_s. It will require a change in the domain shape and volume, which becomes possible since the DMR's cost little energy and there are infinitely many domain configurations that correspond to the same energy even if the magnetostatic energy is also considered. Hence a presence of the parallel χ'_e peak at $T=T_s$ is in principle expected.

The concrete magnetization process needs further study. However, there is one thing which can be visualized: To keep the same domain wall area and change the domain shape and volume, the domain-wall movements should be across a quite large distance. Such movements involve some energy barriers to jump over, which makes the peak present only at low frequencies. These barriers can be due to the intrinsic periodic potential for narrow walls.[23] At 127 K the domain-wall width $\delta_B=2.6$ nm, calculated by Eq. (26) using $K_{\rm eff}=15$ MJ/m^3 and $A=10^{-11}$ J/m. It corresponds to about 15 iron atomic layers. This domain wall is not very narrow, so that the barriers are rather low and can be overcome in the help of thermal activation. The higher the H_{em}, the longer the moving distance. This means that, to have the peak, the frequency should be inversely proportional to H_{em}, which is indeed the experimental result. The domains and walls that can participate in such special movements can only be a small fraction; the absence of a change in the domain-wall area is a very strict condition. If the H_{em} is too high, the main contribution to the DWD susceptibility will be from the major walls, and the peak, which is only due to the special DWD's, must disappear. Since the minimum distance of such wall movements is the lattice constant (because of the periodic potential of narrow walls), the peak will also disappear if H_{em} is too small. Our 0.8-A/m results may belong to this case.

G. Eddy-current effect

Using Eq. (34) and the resistivity given in Ref. 24, $\chi''_{e,\rm eddy}$ is calculated for the perpendicular case of $f=1000$ Hz and $T<T_s$, where the eddy-current effect is the largest. The results are listed in Table I and plotted by solid triangles in Fig. 3(b). For $f\le 100$ Hz, $\chi_{e,\rm eddy}$ is always within the measuring error. Thus all the frequency-dependent χ''_e can be regarded as due to magnetic relaxation, except for the calculated case, where the contribution of eddy currents has to be taken into account.

We see in Fig. 3(b) that the calculated $\chi''_{e,\rm eddy}$ is unreasonably larger than or close to the experimental data for 1000 Hz. The anisotropy in ρ may be one of the reasons. For polycrystals of a compound near $Nd_2Fe_{14}B$, ρ along the c axis is twice as great as that in the basal plane.[25] If the same is true for the present single crystal, then the calculated $\chi''_{e,\rm eddy}$ will decrease by a factor of $\frac{2}{3}$, so that this discrepancy is resolved. Another reason is that $\chi''_{e,\rm eddy}$ is calculated using the experimental χ'_e for 1000 Hz, which includes the contributions from DMR's and DWD's. If the DWD's are due mainly to the closure domain walls, their partial contribution to $\chi''_{e,\rm eddy}$ will be less than calculated from Eq. (34), since the corresponding magnetization is close to the surface. On the contrary, the DMR's are more uniform in the sphere, and Eq. (34) is relevant for them. The fractional DMR makes the real $\chi''_{e,\rm eddy}$ smaller than the calculated one.

In any case the χ''_e for 1000 Hz will be lower after the eddy-current correction. After such a correction, all the curves of χ''_e for $T<T_s$ will correspond to the effect of relaxation.

H. Relaxation

If a relaxation process involves a single time constant τ at a fixed temperature, then, with frequency changing from 0 to ∞, χ'' as a function of the corresponding χ' will draw a half circle starting from $\chi'(f=0)$ and zero χ'' to the $\chi'(f\to\infty)$ and zero χ''.[26] The maximum χ'' corresponds to $2\pi f\tau=1$. A distributed τ makes the half circle oblate, i.e., the maximum χ'' smaller than the half difference between the two extreme values of χ'. However, the average τ can be still estimated by f where a maximum χ'' takes place.

We did not make measurements at a fixed temperature, but from the temperature-dependence curves of χ'' and χ' some analyses can still be made.

In Fig. 3(b) the χ_e'' curves at $T < T_s$ show several peaks or steps. After an eddy-current correction for the data of 1000 Hz, we can make χ_e''-vs-χ_e' functions at different temperatures using the data given in Figs. 3(a) and 3(b). Although there are only three points for each function, two features can still be found: (1) The functions obey not a half-circle type, with the maximum χ_e'' more or less smaller than $[\chi_e'(f \to 0) - \chi_e'(f \to \infty)]/2$; (2) the average τ is between 0.001 and 0.01 s for $T > 40$ K without a monotonical temperature dependence. The first feature means that the relaxation involves a broad or narrow time-constant spectrum, and the second one means that the relaxations at different temperatures are independent, related to different processes.

These processes may be different DWD's enhanced by DMR's. These DWD's will not take place at higher frequencies, which corresponds to a zero χ_e'' and a frequency-independent χ_e'. This will happen for $T < 50$ K at frequencies a little above 1000 Hz, as can be seen from the low-temperature plateau in the χ_e''-vs-T curve of 1000 Hz in Fig. 3(b). Thus the DMR χ_e' in this region should be very close to the 1000-Hz data. In comparison with the three theoretical points in Fig. 3(a), remembering that the vertical DMR susceptibility is mainly due to rotations in the basal plane, we conclude that the real K_3 should be 30% higher than those given in Table I. For $T > 60$ K, χ_e'' is far from zero, so that the DMR χ_e' should be lower than the 1000-Hz curve, and the corresponding K_3 should not vanish. At frequencies lower than 10 Hz, χ_e'' should also decrease, accompanied by an increase in χ_e'.

Another phenomenon which is not easy to understand is for the parallel case, where there exists a broad maximum in χ_e' [Fig. 1(a)] corresponding to a χ_e'' peak [Fig. 1(b)] in the intermediate-temperature region. As treated in Sec. VIII D $k_{\parallel}$ is anomalously increased in this region. Qualitatively, this can be ascribed to the consequence of relaxation, since the maximum decreases with increasing frequency. However, it is not logical for this increment of $k_{\parallel}$ to disappear at higher temperatures. There may be some special mechanism which decreases the K_{eff} in the walls in this region or some DMR's which are related to magnetostatic energy due to a finite sample size.

Further study to understand the parallel susceptibility, including the χ_e' peak at T_s, is in progress.

I. Comments on previous χ derivations

Finally, we would like to comment on some previous works cited in Sec. I that presented some formulas on the initial susceptibilities. For DMR susceptibility parallel to the c axis, our formulas agree with those given in Refs. 15 and 16. However, most authors did not consider (or they neglected) DMR's for the ϕ-angle change, and instead they regarded the DMR susceptibility corresponding to the θ change as the total perpendicular DMR susceptibility. The neglection of the ϕ anisotropy will actually lead to an infinite perpendicular susceptibility at $T < T_s$. Another problem, which makes the solution somewhat arbitrary, is that in some works a magnetostriction term has entered the formula as a positive effective K_1. Actually, this is only valid for a positive magnetostriction constant λ and a positive stress σ along the c axis or when both are negative. In these two cases, however, this effect does not need to be separated from K_1. In any other cases, an inclusion of this effect would drive the solution in confusion. In Table I of Ref. 16, the formulas for [100] and [110] directions have a difference of a factor of 2 without arguments. In our opinion this difference should not appear for the demagnetized state defined in the present work. If magnetic moments are not distributed in all the easy directions with the same probability, the largest difference should be between [110] and [1$\bar{1}$0] directions. There is a typographic error in Ref. 18, where the definition for K should be K_2/K_1.

IX. CONCLUSIONS

The low-field susceptibility of the studied spherical $Nd_2Fe_{14}B$ single crystal is in general due to DMR's and DWD's. Perpendicular to the c axis, χ_e' is dominated by DMR's with respect to the θ angle when $T > T_s$, and it has two comparable contributions from DMR's, mainly with respect to the angle ϕ and from DWD's enhanced by DMR's for $T < T_s$. When $T = T_s$ the perpendicular χ_e' has a maximum of about 2.3, corresponding to an internal χ' larger than 10. Along the c axis, the DWD process is always dominant for χ_e', which is enhanced by DMR's when $T < T_s$ and probably also for $T > T_s$. There is a broad maximum for this χ_e', centered by 190 K, and a χ_e' peak at $T = T_s$ for $f = 1$ and 10 Hz and $H_{em} = 8$–240 A/m. This peak can be ascribed to the cooperation of thermally activated DWD's and nonresistive DMR's within a certain angle. Frequency-dependent χ_e' and χ_e'' are almost totally due to magnetic relaxation processes, which is an important feature of the low-field DWD's. To reach the above conclusions, the low-field DMR susceptibility and 180° domain-wall energy density as functions of anisotropy constants have been derived for different cases. The results can be considered as a basis for the further study of different uniaxially anisotropic single crystals or polycrystals. A formula for the low-frequency eddy-current imaginary susceptibility is derived for a sphere as well. Finally, the spin-reorientation temperature T_s as a characteristic quantity of this material can be determined from temperature-dependent low-field ac susceptibility measurements through (1) the sharp peak of $\chi_e'(\perp)$, (2) the sharp onset of $\chi_e''(\perp)$ from zero, (3) the sharp peak of $\chi_e'(\parallel)$ at $H_{em} = 8$ A/m and $f = 10$ Hz, and (4) the dip of $\chi_e'(\parallel)$ at $H_{em} \geq 80$ A/m. A precise result, 127 K, is obtained by the former three approaches.

ACKNOWLEDGMENTS

The authors would like to thank R. Vatter for help in setting up the ac susceptometer and W.-J. Qiang, I. Kleinschroth, and G. Martinek for helpful discussion.

*On leave from Physics Department, Universitat Autònoma Barcelona, 08193 Bellaterra, Spain; present address: Instituto de Magnetismo Aplicado, RENFE-UCM, Las Rozas, Madrid, Spain.

[1]D. Givord, H. S. Li, and R. Perrier de la Bathie, Solid State Commun. **51**, 857 (1984).

[2]M. Sagawa, S. Fujimura, H. Yamamoto, Y. Matsuura, and H. Hirosawa, J. Appl. Phys. **57**, 4095 (1985).

[3]O. Yamada, H. Tokuhara, F. Ono, M. Sagawa, and Y. Matsuura, J. Magn. Magn. Mater. **54-57**, 585 (1986).

[4]Y. Otani, H. Miyajima, and S. Chikazumi, J. Appl. Phys. **61**, 3436 (1987).

[5]J. M. Cadogan, J. P. Gavigan, D. Givord, and H. S. Li, J. Phys. F. **18**, 779 (1988).

[6]S. Hock, Ph.D. thesis, Max-Plank-Institut für Metallforschung, Institut für Physik, 1988.

[7]G. C. Hadjipanayis, K. R. Lawiess, and R. C. Dickerson, J. Appl. Phys. **57**, 4097 (1985).

[8]R. Graessinger, X. S. Sun, R. Eibler, K. H. J. Buschow, and H. R. Kirchmayr, J. Magn. Magn. Mater. **58**, 55 (1986).

[9]M. R. Ibarra, C. Marquina, P. A. Algarabel, J. I. Arnaudas, and A. del Moral, J. Appl. Phys. **64**, 5537 (1988).

[10]M. R. Ibarra, C. Marquina, P. A. Algarabel, J. I. Arnaudas, and A. del Moral, Solid State Commun. **69**, 131 (1989).

[11]A. del Moral, M. R. Ibarra, C. Marquina, J. I. Arnaudas, and P. A. Algarabel, J. Magn. Magn. Mater. **83**, 283 (1990).

[12]S. K. Malik, D. T. Adroja, B. M. Ma, E. B. Boltich, J. G. Sohn, S. G. Sankar, and W. E. Wallace, J. Appl. Phys. **67**, 4589 (1990).

[13]Bo-Ping Hu, Hong-Shuo Li, Hong Sun, J. F. Lawler, and J. M. D. Coey, Solid State Commun. **76**, 587 (1990).

[14]X. C. Kou and R. Graessinger, J. Magn. Magn. Mater. **95**, 184 (1991).

[15]P. A. Algarabel, A. del Moral, M. R. Ibarra, and J. I. Arnaudas, J. Phys. Chem. Solids **49**, 213 (1988).

[16]C. Rillo, J. Chaboy, R. Navarro, J. Bartonomé, D. Fruchart, B. Chenevier, A. Yaouanc, M. Sagawa, and S. Hirosawa, J. Appl. Phys. **64**, 5534 (1988).

[17]F. J. Lazaro, J. Bartolomé, R. Navarro, C. Rillo, F. Lera, L. M. Garcia, J. Chaboy, C. Pique, R. Burriel, D. Fruchart, and S. Miraglia, J. Magn. Magn. Mater. **83**, 289 (1990).

[18]M. Foldeaki, L. Koszegi, and R. A. Dunlap, J. Magn. Magn. Mater. **96**, 29 (1991).

[19]H. U. Aström, D.-X. Chen, G. Benediktsson, and K. V. Rao, J. Phys. Condens. Matter **2**, 3349 (1990).

[20]D.-X. Chen, *Ballistic and Bridge Methods of Magnetic Measurements of Materials* (China Metrology, Beijing, 1990), p. 526.

[21]D. J. Craik and R. S. Tebble, *Ferromagnetism and Ferromagnetic Domains* (North-Holland, Amsterdam, 1965), pp. 26 and 43.

[22]R. Carey and E. D. Isaac, *Magnetic Domains and Techniques for Their Observation* (English Universities Press, London, 1966), p. 18.

[23]H. R. Hilzinger and H. Kronmüler, Phys. Status Solidi B **54**, 593 (1972).

[24]J. B. Sousa, M. M. Amado, R. P. Pinto, V. S. Amaral, and M. E. Braga, J. Phys. Condens. Matter **2**, 7543 (1990).

[25]M. A. Sa, J. M. Machado da Silva, and J. B. Oliveira (unpublished).

[26]A. J. van Duyneveldt, J. Appl. Phys. **53**, 8006 (1982).